SARS-CoV-2 protein ORF3a is pathogenic in *Drosophila* and causes phenotypes associated with COVID-19 post-viral syndrome

Shuo Yang[1], Meijie Tian[2], and Aaron N. Johnson[1,3]

[1]Department of Developmental Biology
Washington University School of Medicine
St. Louis, MO 63110

[2]Genetics Branch, Oncogenomics Section
National Cancer Institute, NIH
Bethesda, MD 20892

[3]Author for correspondence: anjohnson@wustl.edu

Highlights

SARS-CoV-2 ORF3a is pathogenic in the nervous system.

ORF3a induces cell death, inflammation, and lysosome dysfunction.

Chloroquine protects against ORF3a induced CNS distress and lysosome dysfunction.

Summary

The Coronavirus Disease 2019 (COVID-19) pandemic has caused millions of deaths and will continue to exact incalculable tolls worldwide. While great strides have been made toward understanding and combating the mechanisms of Severe Acute Respiratory Syndrome Coronavirus-2 (SARS-CoV-2) infection, relatively little is known about the individual SARS-CoV-2 proteins that contribute to pathogenicity during infection and that cause neurological sequela after viral clearance. We used *Drosophila* to develop an *in vivo* model that characterizes mechanisms of SARS-CoV-2 pathogenicity, and found ORF3a adversely affects longevity and motor function by inducing apoptosis and inflammation in the nervous system. Chloroquine alleviated ORF3a induced phenotypes in the CNS, arguing our *Drosophila* model is amenable to high throughput drug screening. Our work provides novel insights into the pathogenic nature of SARS-CoV-2 in the nervous system that can be used to develop new treatment strategies for post-viral syndrome.

Main Text

SARS-CoV-2 is the causative agent of the ongoing COVID-19 pandemic, which has resulted in more than 1.5 million deaths worldwide (JHU, 2020). To stem the spread of SARS-CoV-2 and control the COVID-19 pandemic, SARS-CoV-2 research has primarily focused on understanding the mechanisms of viral infection and transmission. For example, ACE2 encodes a SARS-CoV-2 receptor, and humanized ACE2 transgenic mice have been developed to investigate the mechanisms of SARS-CoV-2 infection *in vivo* (Jiang et al., 2020; Kim et al., 2020; Sun et al., 2020). In contrast, relatively little is known about how specific SARS-CoV-2 proteins induce pathogenesis (Kumar et al., 2020). The high COVID-19 mortality rate suggests that proteins encoded by the SARS-CoV-2 genome are unusually virulent. After the active SARS-CoV-2 infection is cleared, or no longer detectable, a majority of recovering patients will experience post viral syndrome with indications that include neuropsychiatric symptoms and extreme fatigue lasting for several months (Mooney et al., 2020; Townsend and Dyer, 2020). As recently developed vaccines begin to control the COVID-19 pandemic, it will be critically important to identify the mechanisms by which SARS-CoV-2 proteins cause pathogenesis in order to develop treatments that mitigate the adverse affects associated with the sequela of infection.

The SARS-Cov-2 genome encodes 11 genes with 14 open reading frames (ORFs), that produce a total of 29 proteins including 16 nonstructural proteins (NSP1-NSP16), 4 structural proteins (spike protein [S)], membrane protein [M], nucleocapsid protein [N], envelope protein [E]), and 9 accessory proteins (ORF3a, ORF3b, ORF6, ORF7a, ORF7b, ORF8, ORF9b, ORF9c and ORF10)(Gordon et al., 2020). The ORF3a protein is unique to coronaviruses and has been characterized in SARS-CoV, which caused the severe acute respiratory syndrome (SARS) outbreak in 2003. SARS-CoV ORF3a triggers a pathogenic inflammatory reaction through its interaction with TRAF3 that drives IL-1/IL-18 maturation and ultimately causes severe lung damage through cell pyroptosis and apoptosis (Siu et al., 2019). Moreover, SARS-CoV ORF3a induces vesicle formation and golgi fragmentation, which are prominent features observed in patient samples (Freundt et al., 2010). SARS-CoV-2 ORF3a might also be pathogenic. *In vitro* studies show SARS-CoV-2 ORF3a induces caspase-dependent apoptosis (Ren et al., 2020), while *in silico* studies argue that the ORF3a mutation rate directly correlates with SARS-CoV-2 mortality rates after infection (Majumdar and Niyogi, 2020). In addition, SARS-CoV-2 ORF3a facilitates virus replication by high jacking the autophagy machinery; despite 72.36% amino acid identity between the ORF3a proteins (Fig. S1A), SARS-CoV ORF3a does not promote viral replication (Qu et al., 2020). Although these studies suggest that SARS-CoV-2 ORF3a has unique pathogenic functions that contribute to the relatively high COVID-19 mortality rate, an *in vivo* model has yet to be developed that specifically interrogates the mechanisms of SARS-CoV-2 ORF3a pathogenicity.

To date, clinical treatments are not available that alleviate SARS-CoV-2 post viral syndrome. Identifying drugs that treat COVID-19 remains an urgent need, but the low availability of hACE2 transgenic mice and the requirement for P3-level infrastructure to handle SARS-CoV-2 viruses prevents a vast majority of laboratories from conducting COVID-19 research. An alternative strategy is to develop *in vivo* models of SARS-CoV-2 pathogenicity in which candidate drugs targeting specific viral proteins can be tested for protection against pathogenic outcomes. Promising therapeutic strategies would include compounds that block hyperinflammation and apoptosis induced by pathogenic viral proteins (Freeman and Swartz, 2020; van den Berg and Te Velde, 2020; Yap et al., 2020).

The powerful genetic tools in *Drosophila* have been used to identify essential mechanisms that

underlie viral infections (Hao et al., 2008; Hughes et al., 2012; Yang et al., 2018), and that contribute to viral pathogenicity (Adamson et al., 2011; Chan et al., 2009; Harsh et al., 2020). In addition, the short lifespan with easy-to-score visible phenotypes has made the fruit fly a productive *in vivo* drug screening platform (Chang et al., 2008; Dar et al., 2012; Su, 2019; Willoughby et al., 2013). Here, we report the development and characterization of an *in vivo Drosophila* model that assays SARS-CoV-2 proteins for tissue-specific pathogenicity and that can successfully identify drug candidates that mitigate pathogenic SARS-CoV-2 proteins.

We constructed a transgenic fly that placed ORF3a under UAS control. SARS-CoV-2 infection shows a strong tissue preference, most notably affecting the respiratory system, due to the usual route of infection and the relative abundance of ACE2 among tissues (Hikmet et al., 2020; Puelles et al., 2020). To understand if SARS-CoV-2 pathogenicity can also be tissue-specific, we used the bipartite GAL4/UAS system to express ORF3a in the central nervous system (CNS; *elav.Gal4*), in photoreceptors (*GMR.Gal4*), and in striated and smooth muscle (*Mef2.Gal4*). Each Gal4 driver robustly induced ORF3a expression (Fig. 1A, S1B,C), but appreciable phenotypes were only observed in flies that expressed ORF3a in the nervous system. ORF3a expression in the CNS significantly reduced lifespan (control median survival>14d, n=60; *elav>ORF3a*=5.0d, n=65; Fig 1B), impaired motor function in longitudinal climbing assays (average performance *elav>ORF3a* =1.9% of control, n>60 per genotype; Fig. 1C, S1D), and induced pronounced abdominal swelling (>90% individuals, n=65, Fig. S1E). Fewer *elav>ORF3a* adult flies eclosed than expected (49.5% of expected, n=188; Fig. 1D), suggesting ORF3a caused partial lethality during larval stages. In addition, flies that expressed ORF3a in photoreceptors showed a rough eye phenotype, which is consistent with defects in ommatidia patterning and apoptosis (100% affected, n>100; Fig. 1E). Surprisingly, ORF3a expression in muscle did not significantly affect longevity, motor function, or muscle patterning (Fig. 1F, S1F). Consistent with these results, >35% of COVID-19 patients showed neurological symptoms whereas <10% of patients showed musculoskeletal complications (Mao et al., 2020). These studies argue that ORF3a is pathogenic in only a subset of tissues, and that the CNS is particularly sensitive to ORF3a expression.

After establishing a primary infection in the respiratory system, SARS-CoV and SARS-CoV-2 can

pass the blood-brain barrier and efficiently infect the CNS (Glass et al., 2004; Meinhardt et al., 2020; Puelles et al., 2020; Zheng et al., 2020), and SARS-CoV-2 has been associated with a host of neurological symptoms including impaired consciousness, stroke, concentration problems, memory loss, dizziness and insomnia (Mao et al., 2020). Reduced lifespan and impaired motor function in *elav>ORF3a* flies are phenotypes indicative of neurodegeneration (Moore et al., 2018), so we assessed apoptosis in the adult brain, and found that ORF3a induced Caspase-3 cleavage (Fig. 1G). Neuroinflammation is often seen in COVID-19 patients, possibly via damage-associated molecular patterns (DAMPs) induced TLR4-MyD88 signaling activation (Meinhardt et al., 2020; Ren et al., 2020; Zhou et al., 2020). In *Drosophila*, non-infectious sterile inflammation can be initiated when necrotic cells release DAMPs that in turn activate immunoinflammatory pathways, including the Toll and IMD pathways (Kosakamoto et al., 2020; Obata et al., 2014). We hypothesized that ORF3a elicits a sterile inflammatory response, and found that expressing ORF3a in the CNS induced Toll pathway reporter expression (fold change vs control, *Drs*=10.2; Fig. 1H) and IMD reporter expression (*dipt*=28.8, *attA*=55.9)(Yang et al., 2019). We also assayed *eiger* expression, which is a marker for Jun kinase (JNK)-mediated inflammation and apoptosis (Li et al., 2019), but *eiger* expression was not significantly changed in *elav>ORF3a* flies (Fig. 1I). These data demonstrate that ORF3a expression alone is sufficient to cause apoptosis, neuroinflammation, and neurotropism, and suggest ORF3a is a major virulence factor of SARS-CoV-2. Thus our ORF3a transgenic fly model recapitulates hallmarks of SARS-CoV-2 infection reported in patients and cell culture systems.

We next wanted to understand if our ORF3a model could be used to identify COVID-19 treatments. In Vero cells, lysosome deacidification is essential for virus egress, and ORF3a localized to lysosomes and caused lysosome deacidification (Ghosh et al., 2020). Toxic stress also caused lysosome deacidification in U2OS cells, and chloroquine phosphate (CQ) blocked chemically induced deacidification (Mauthe et al., 2018). Although CQ did not consistently prevent SARS-CoV-2 infections in clinical trials, the ORF3a lysosome studies suggested that CQ could prevent ORF3a-induced tropism. To understand if our fly model could respond to COVID-19 treatments, we tested the efficacy of CQ in mitigating ORF3a phenotypes. CQ treated *elav>ORF3a* flies showed significantly longer lifespans

(*elav>ORF3a* median survival=6d, n=121; *elav>ORF3a*+CQ=14d, n=79; Fig 2A), and improved motor function compared to untreated controls (average performance *elav>ORF3a*=1.3% of control; *elav>ORF3a*+CQ=9.8% of control; n>60 per genotype; Fig 2B). In addition, more CQ treated *elav>ORF3a* adult flies eclosed than untreated controls (treated=72.4% of expected, n=174; untreated=49.5%; Fig. 2C), suggesting CQ can suppress ORF3a induced larval lethality. These proof of principle studies largely validate our ORF3a *Drosophila* model as an efficient COVID-19 drug-screening platform.

At the molecular level, CQ treated *elav>ORF3a* flies showed reduced cleaved-caspase-3 levels (untreated FC=2.3; treated FC=1.3; Figure 2D), and reduced Toll pathway activity (*Drs;* FC=0.43 vs untreated; Fig. 2E) compared to untreated controls. However, IMD pathway reporters did not respond to CQ treatment (*dipt*=0.75, *attA*=0.89). One mechanism that might explain CQ specificity is that the Toll pathway is a more direct target of necrotic derived DAMPs, while the IMD pathway is not (Kosakamoto et al., 2020). A second mechanism of action for CQ could involve ORF3a-induced lysosome dysfunction. LysoTracker is a vital dye that accumulates in acidic organelles and is often used as a marker for lysosome function (Sanman et al., 2016). Similar to Vero cells, ORF3a promoted lysosome deacidification in HeLa cells (Fig. 2G,H). Strikingly, we found CQ treatment efficiently blunted ORF3a induced deacidification (Fig. 2G,H). While CQ showed no effect on inpatient survival (Geleris et al., 2020), our results argue CQ prevents apoptosis and lysosome dysfunction in ORF3a-expressing cells, and suggest CQ could ameliorate symptoms associated with SARS-CoV-2 post viral syndrome in recovering patients (Fig. 2I).

The sequela of SARS-CoV-2 infection includes extensive neurological complications such as problems with concentration, memory loss, anxiety and depression (Halpin et al., 2020). Since the duration and severity of persistent symptoms among COVID-19 survivors is continuing to emerge, understanding and treating COVID-19 post viral syndrome will be a high healthcare priority over the next several years. Time course studies of SARS-CoV-2 infection, replication, and clearance have yet to be reported in detail, but infection parameters have been defined for the closely related SARS-CoV in mice (Glass et al., 2004). SARS-CoV was detectable in the lungs for up to 9 days after an initial nasal

inoculation, and then spread to the CNS where the virus was detectable for an additional 6 days (Glass et al., 2004). Interestingly, after infectious SARS-CoV, SARS-CoV-2, and the coronavirus Middle East Respiratory Syndrome (MERS)-CoV has been cleared, viral RNA continues to be detectable in many tissues (Glass et al., 2004; Sia et al., 2020; Widagdo et al., 2019).

Our study revealed ORF3a expression in the nervous system alone can induce cell death and neuroinflammation, suggesting ORF3a is the major virulence factor contributing to SARS-CoV-2 induced neurotropism (Figs. 1B,C). In addition, the gold standard PCR-based SARS-CoV-2 test can only assess viral load in the respiratory system. After SARS-CoV-2 is cleared from the respiratory system, and a patient tests negative, SARS-CoV-2 may continue to replicate in the CNS (Fig. 2J). The residual ORF3a may continue to trigger neurological complications associated with post viral syndrome in recovering patients, suggesting continued medical treatments are in fact required for full recovery after a 'negative' PCR-based SARS-CoV-2 test.

In summary, our results warrant further studies of SARS-CoV-2 pathogenic mechanisms as a means to treat COVID-19 post viral syndrome and identify ORF3a as a high priority target that is amenable to drug treatment (Fig. 2A,B). A future drug screen with ORF3a transgenic flies will likely reveal post-viral syndrome treatments beyond CQ.

Acknowledgments

We thank Jennifer McAdow, Yingqiu Du, and Tiffany Ou for technical support throughout the project. We also thank Mayssa Mokalled for the relentless encouragement. ANJ was supported by NIH R01AR070299.

Author Contributions

Conceptualization, S.Y., M.T. and ANJ.; Methodology and Validation, S.Y.; Formal Analysis, S.Y., M.T., and ANJ.; Investigation, S.Y. and M.T.; Resources, ANJ.; Writing-Original Draft, S.Y., M.T. and ANJ.; Supervision, ANJ.; Funding Acquisition, ANJ.

Declaration Of Interests

The authors declare no competing interests.

References

Adamson, A.L., Chohan, K., Swenson, J., and LaJeunesse, D. (2011). A Drosophila model for genetic analysis of influenza viral/host interactions. Genetics *189*, 495-506.

Chan, C.M., Tsoi, H., Chan, W.M., Zhai, S., Wong, C.O., Yao, X., Chan, W.Y., Tsui, S.K., and Chan, H.Y. (2009). The ion channel activity of the SARS-coronavirus 3a protein is linked to its pro-apoptotic function. Int J Biochem Cell Biol *41*, 2232-2239.

Chang, S., Bray, S.M., Li, Z., Zarnescu, D.C., He, C., Jin, P., and Warren, S.T. (2008). Identification of small molecules rescuing fragile X syndrome phenotypes in Drosophila. Nat Chem Biol *4*, 256-263.

Dar, A.C., Das, T.K., Shokat, K.M., and Cagan, R.L. (2012). Chemical genetic discovery of targets and anti-targets for cancer polypharmacology. Nature *486*, 80-84.

Freeman, T.L., and Swartz, T.H. (2020). Targeting the NLRP3 Inflammasome in Severe COVID-19. Front Immunol *11*, 1518.

Freundt, E.C., Yu, L., Goldsmith, C.S., Welsh, S., Cheng, A., Yount, B., Liu, W., Frieman, M.B., Buchholz, U.J., Screaton, G.R., *et al.* (2010). The open reading frame 3a protein of severe acute respiratory syndrome-associated coronavirus promotes membrane rearrangement and cell death. J Virol *84*, 1097-1109.

Geleris, J., Sun, Y., Platt, J., Zucker, J., Baldwin, M., Hripcsak, G., Labella, A., Manson, D.K., Kubin, C., Barr, R.G., *et al.* (2020). Observational Study of Hydroxychloroquine in Hospitalized Patients with Covid-19. N Engl J Med *382*, 2411-2418.

Ghosh, S., Dellibovi-Ragheb, T.A., Kerviel, A., Pak, E., Qiu, Q., Fisher, M., Takvorian, P.M., Bleck, C., Hsu, V.W., Fehr, A.R., *et al.* (2020). beta-Coronaviruses Use Lysosomes for Egress Instead of the Biosynthetic Secretory Pathway. Cell.

Glass, W.G., Subbarao, K., Murphy, B., and Murphy, P.M. (2004). Mechanisms of host defense following severe acute respiratory syndrome-coronavirus (SARS-CoV) pulmonary infection of mice. J Immunol *173*, 4030-4039.

Gordon, D.E., Jang, G.M., Bouhaddou, M., Xu, J., Obernier, K., White, K.M., O'Meara, M.J., Rezelj, V.V., Guo, J.Z., Swaney, D.L., *et al.* (2020). A SARS-CoV-2 protein interaction map reveals targets for drug repurposing. Nature *583*, 459-468.

Halpin, S.J., McIvor, C., Whyatt, G., Adams, A., Harvey, O., McLean, L., Walshaw, C., Kemp, S., Corrado, J., Singh, R., *et al.* (2020). Postdischarge symptoms and rehabilitation needs in survivors of COVID-19 infection: A cross-sectional evaluation. Journal of Medical Virology *n/a*.

Hao, L., Sakurai, A., Watanabe, T., Sorensen, E., Nidom, C.A., Newton, M.A., Ahlquist, P., and Kawaoka, Y. (2008). Drosophila RNAi screen identifies host genes important for influenza virus replication. Nature *454*, 890-893.

Harsh, S., Fu, Y., Kenney, E., Han, Z., and Eleftherianos, I. (2020). Zika virus non-structural protein NS4A restricts eye growth in Drosophila through regulation of JAK/STAT signaling. Dis Model Mech *13*.

Hikmet, F., Mear, L., Edvinsson, A., Micke, P., Uhlen, M., and Lindskog, C. (2020). The protein expression profile of ACE2 in human tissues. Mol Syst Biol *16*, e9610.

Hughes, T.T., Allen, A.L., Bardin, J.E., Christian, M.N., Daimon, K., Dozier, K.D., Hansen, C.L., Holcomb, L.M., and Ahlander, J. (2012). Drosophila as a genetic model for studying pathogenic human viruses. Virology *423*, 1-5.

JHU (2020). Johns Hopkins Coronavirus Resource Center.

Jiang, R.D., Liu, M.Q., Chen, Y., Shan, C., Zhou, Y.W., Shen, X.R., Li, Q., Zhang, L., Zhu, Y., Si, H.R., *et al.* (2020). Pathogenesis of SARS-CoV-2 in Transgenic Mice Expressing Human Angiotensin-Converting Enzyme 2. Cell *182*, 50-58 e58.

Kim, Y.I., Kim, S.G., Kim, S.M., Kim, E.H., Park, S.J., Yu, K.M., Chang, J.H., Kim, E.J., Lee, S., Casel, M.A.B., *et al.* (2020). Infection and Rapid Transmission of SARS-CoV-2 in Ferrets. Cell Host Microbe *27*, 704-709 e702.

Kosakamoto, H., Yamauchi, T., Akuzawa-Tokita, Y., Nishimura, K., Soga, T., Murakami, T., Mori, H., Yamamoto, K., Miyazaki, R., Koto, A.*, et al.* (2020). Local Necrotic Cells Trigger Systemic Immune Activation via Gut Microbiome Dysbiosis in Drosophila. Cell Rep *32*, 107938.

Kumar, A., Prasoon, P., Kumari, C., Pareek, V., Faiq, M.A., Narayan, R.K., Kulandhasamy, M., and Kant, K. (2020). SARS-CoV-2-specific virulence factors in COVID-19. J Med Virol.

Li, M., Sun, S., Priest, J., Bi, X., and Fan, Y. (2019). Characterization of TNF-induced cell death in Drosophila reveals caspase- and JNK-dependent necrosis and its role in tumor suppression. Cell death & disease *10*, 613.

Majumdar, P., and Niyogi, S. (2020). ORF3a mutation associated higher mortality rate in SARS-CoV-2 infection. Epidemiol Infect, 1-16.

Mao, L., Jin, H., Wang, M., Hu, Y., Chen, S., He, Q., Chang, J., Hong, C., Zhou, Y., Wang, D.*, et al.* (2020). Neurologic Manifestations of Hospitalized Patients With Coronavirus Disease 2019 in Wuhan, China. JAMA Neurol *77*, 683-690.

Mauthe, M., Orhon, I., Rocchi, C., Zhou, X., Luhr, M., Hijlkema, K.J., Coppes, R.P., Engedal, N., Mari, M., and Reggiori, F. (2018). Chloroquine inhibits autophagic flux by decreasing autophagosome-lysosome fusion. Autophagy *14*, 1435-1455.

Meinhardt, J., Radke, J., Dittmayer, C., Franz, J., Thomas, C., Mothes, R., Laue, M., Schneider, J., Brünink, S., Greuel, S.*, et al.* (2020). Olfactory transmucosal SARS-CoV-2 invasion as a port of central nervous system entry in individuals with COVID-19. Nature neuroscience.

Mooney, A., Gaffney, F., Jones, K., Dunne, J., O'Connor, L., Leavy, D., O'Brien, K., Dowds, J., Sugrue, J.A., Hopkins, D.*, et al.* (2020). PLoS One.

Moore, B.D., Martin, J., de Mena, L., Sanchez, J., Cruz, P.E., Ceballos-Diaz, C., Ladd, T.B., Ran, Y., Levites, Y., Kukar, T.L.*, et al.* (2018). Short Abeta peptides attenuate Abeta42 toxicity in vivo. J Exp Med *215*, 283-301.

Obata, F., Kuranaga, E., Tomioka, K., Ming, M., Takeishi, A., Chen, C.H., Soga, T., and Miura, M. (2014). Necrosis-driven systemic immune response alters SAM metabolism through the FOXO-GNMT axis. Cell Rep *7*, 821-833.

Puelles, V.G., Lutgehetmann, M., Lindenmeyer, M.T., Sperhake, J.P., Wong, M.N., Allweiss, L., Chilla, S., Heinemann, A., Wanner, N., Liu, S.*, et al.* (2020). Multiorgan and Renal Tropism of SARS-CoV-2. N Engl J Med *383*, 590-592.

Qu, Y., Wang, X., Zhu, Y., Wang, Y., Yang, X., Hu, G., Liu, C., Li, J., Ren, S., Xiao, Z.*, et al.* (2020). ORF3a mediated-incomplete autophagy facilitates SARS-CoV-2 replication. bioRxiv, 2020.2011.2012.380709.

Ren, Y., Shu, T., Wu, D., Mu, J., Wang, C., Huang, M., Han, Y., Zhang, X.Y., Zhou, W., Qiu, Y.*, et al.* (2020). The ORF3a protein of SARS-CoV-2 induces apoptosis in cells. Cell Mol Immunol *17*, 881-883.

Sanman, L.E., van der Linden, W.A., Verdoes, M., and Bogyo, M. (2016). Bifunctional Probes of Cathepsin Protease Activity and pH Reveal Alterations in Endolysosomal pH during Bacterial Infection. Cell chemical biology *23*, 793-804.

Sia, S.F., Yan, L.M., Chin, A.W.H., Fung, K., Choy, K.T., Wong, A.Y.L., Kaewpreedee, P., Perera, R., Poon, L.L.M., Nicholls, J.M.*, et al.* (2020). Pathogenesis and transmission of SARS-CoV-2 in golden hamsters. *583*, 834-838.

Siu, K.L., Yuen, K.S., Castano-Rodriguez, C., Ye, Z.W., Yeung, M.L., Fung, S.Y., Yuan, S., Chan, C.P., Yuen, K.Y., Enjuanes, L.*, et al.* (2019). Severe acute respiratory syndrome coronavirus ORF3a protein activates the NLRP3 inflammasome by promoting TRAF3-dependent ubiquitination of ASC. FASEB J *33*, 8865-8877.

Su, T.T. (2019). Drug screening in Drosophila; why, when, and when not? Wiley Interdiscip Rev Dev Biol *8*, e346.

Sun, S.H., Chen, Q., Gu, H.J., Yang, G., Wang, Y.X., Huang, X.Y., Liu, S.S., Zhang, N.N., Li, X.F., Xiong, R.*, et al.* (2020). A Mouse Model of SARS-CoV-2 Infection and Pathogenesis. Cell Host Microbe *28*, 124-133 e124.

Townsend, L., and Dyer, A.H. (2020). Persistent fatigue following SARS-CoV-2 infection is common and independent of severity of initial infection. *15*, e0240784.

van den Berg, D.F., and Te Velde, A.A. (2020). Severe COVID-19: NLRP3 Inflammasome Dysregulated. Front Immunol *11*, 1580.

Widagdo, W., Sooksawasdi Na Ayudhya, S., Hundie, G.B., and Haagmans, B.L. (2019). Host Determinants of MERS-CoV Transmission and Pathogenesis. Viruses *11*.

Willoughby, L.F., Schlosser, T., Manning, S.A., Parisot, J.P., Street, I.P., Richardson, H.E., Humbert, P.O., and Brumby, A.M. (2013). An in vivo large-scale chemical screening platform using Drosophila for anti-cancer drug discovery. Dis Model Mech *6*, 521-529.

Yang, S., Yu, J., Fan, Z., Gong, S.T., Tang, H., and Pan, L. (2018). Bub1 Facilitates Virus Entry through Endocytosis in a Model of Drosophila Pathogenesis. J Virol *92*.

Yang, S., Zhao, Y., Yu, J., Fan, Z., Gong, S.T., Tang, H., and Pan, L. (2019). Sugar Alcohols of Polyol Pathway Serve as Alarmins to Mediate Local-Systemic Innate Immune Communication in Drosophila. Cell Host Microbe *26*, 240-251 e248.

Yap, J.K.Y., Moriyama, M., and Iwasaki, A. (2020). Inflammasomes and Pyroptosis as Therapeutic Targets for COVID-19. J Immunol *205*, 307-312.

Zheng, J., Wong, L.R., Li, K., Verma, A.K., Ortiz, M.E., Wohlford-Lenane, C., Leidinger, M.R., Knudson, C.M., Meyerholz, D.K., McCray, P.B., Jr.*, et al.* (2020). COVID-19 treatments and pathogenesis including anosmia in K18-hACE2 mice.

Zhou, T., Su, T.T., Mudianto, T., and Wang, J. (2020). Immune asynchrony in COVID-19 pathogenesis and potential immunotherapies. J Exp Med *217*.

Materials and methods

Drosophila genetics

The Gal4 stocks used to express SARS-CoV-2 ORF3a in brain, eye, and muscle included P{GAL4-elav.L} (Bloomington Stock Center, 8760), P{GAL4-ninaE.GMR} (Bloomington Stock Center, 1104), and P{Mef2-GAL4.247} (Bloomington Stock Center, 50742). Flies were maintained on standard "Bloomington recipe" media, and cultured at 25 °C under a normal light/dark cycle, unless otherwise noted.

Transgenic Flies

UAS-SARS-CoV-2-ORF3a transgenic flies were generated by PCR-mediated subcloning of the SARS-CoV-2-ORF3a coding sequence (pDONR207 SARS-CoV-2 ORF3A, #141271, Addgene) into pUASt-Attb (EcoRI/XbaI). ORF3a was amplified with Takara PrimerSTAR PCR enzyme (R050B, Takara) using the following primers:

ORF3a-CDS-Forward- CGGAATTCATGGACCTGTTCATGAGAATCTT

ORF3a-CDS-Rerverse-GCTCTAGATTACAGTGGCACGGAGGTG

Plasmid DNA was injected and targeted to a C31 integration site at 22A2 (Bloomington Stock 24481, Rainbow Transgenic Flies); stable insertions were identified by standard methods.

Immunohistochemistry and imaging

Antibodies used include anti-SARS-CoV-2-ORF3a (1:200, 101AP, FabGennix International Inc), anti-Tropomyosin (1:600, MAC141, Abcam). Embryo and brain antibody staining was performed as described (Yang et al., 2019). Tissues were imaged with a Zeiss LSM800 confocal microscope. For *Drosophila* eye imaging, *UAS-ORF3a/TM3, Sb* flies were crossed with *GMR-gal4* virgin flies to direct expression of ORF3a in eyes. For wild type control, w^{1118} flies were crossed with *GMR-gal4* virgin flies. Flies were crossed at 25°C for two days; the progeny were raised at 29°C, and female adults were collected at day 3 post eclosure. Flies were frozen at −80°C for at least 24 h and imaged with a ZEISS Axio Zoom V16 Microscope. Projected in-focus images were produced with the Montage Multifocus module of the Zen Pro Software.

Cell culture

pCMV-GFP-SARS-CoV-ORF3a was generated by recombining the SARS-CoV-2-ORF3a coding sequence (pDONR207 SARS-CoV-2 ORF3A, #141271, Addgene) into pDEST-CMV-N-EGFP (#122842, Addgene). For LysoTracker staining, Hela cells were seeded in 6-well plates with cover slips and grown to 50% confluency at 37°C with 5%CO2 in Dulbecco's modified Eagle's medium (12430047, Invitrogen) supplemented with 10% heat-inactivated FBS (A4766801, Invitrogen). Cells were then transfected with 1000ng DNA, using standard Lipofectamine 3000 protocols (L3000008, Invitrogen). Media was changed to DMEM with or without 10 μM chloroquine diphosphate (C6628, Sigma) 6h post transfection. 24h latter, media was removed, and cells were incubated with 10 nM LysoTracker Red DND-99 (L7528, Invitrogen) for 1h. Cells was washed with PBS for three times, mounted and imaged with a Zeiss LSM800 confocal microscope.

Western blotting

For each sample, 10 adult female heads were homogenized in 200 μl IP buffer (20 mM Hepes, pH=7.4, 150 nM NaCl, 1% NP40, 1.5 mM MgCl2, 2 mM EGTA, 10 mM NaF, 1 mM Na3VO4, 1X proteinase inhibitor), incubated on ice for 30 min and large debris was removed by 15min centrifugation (12,000Xg). Anti-cleaved-caspase 3 (#9661, Cell Signaling Technology) and anti-beta-actin (E7-C, DSHB) were used for immunoblotting. Western blots were performed by standard method using precast gels (#456-1096, BioRad), and imaged with the ChemiDoc XRS+ system (BioRad).

Longevity and motor function assays

1d old adult flies were collected and transferred to fresh food daily for both assays. For longevity analysis, the number of dead flies was recorded daily. Kaplan-Meier survival curves were generated, and statistical analysis was performed using log-rank analysis (Prism9, GraphPad Software). To assess motor function climbing assays were performed at described (Moore et al., 2018). Briefly, 15-20 flies were placed into empty vials (9.5 cm high,1.7 cm in diameter) with flat bottoms, the flies were forced to the bottom of a vial by firmly tapping the vial against the bench surface. Eight seconds after the tap, the number of flies that climbed up the walls of a vial above the 5-cm mark was recorded as positive.

in vivo drug treatment

40mg/ml chloroquine phosphate (CQ, Sigma, C6628) was dissolved in water, and 40mg of CQ was added to each 30g of fresh fly media. Adult flies were placed on treated food at 25°C for 2d and then transferred. Progeny were cultured on CQ food from embryo stage to eclosion and transferred 24hr later to normal media (to prevent adults from sticking to wet, treated media).

Quantitative real-time RT-PCR

Total RNA was extracted with TRIzol (15596026, Invitrogen), and quantitated with a Nanodrop 2000 (Thermo Fisher). cDNA was prepared by reverse transcription with All-in-One 5X RT MasterMix (G592, Applied Biological Materials Inc) with 1000ng RNA. BlasTaq 2X qPCR MasterMix (G891, Applied Biological Materials Inc) and ABI Step One system (Applied Biosystems) were used for quantitative RT-PCR. Quantification was normalized to endogenous ribosomal protein Rp32 mRNA. RT-PCR primers included:

Diptercin-F: GGCTTATCCGATGCCCGACG

Diptercin-R: TCTGTAGGTGTAGGTGCTTCCC

Attacin-A-F: ACGCCCGGAGTGAAGGATGTT

Attacin-A-R: GGGCGATGACCAGAGATTAGCAC

Drosomycin-F: GCAGATCAAGTACTTGTTCGCCC

Drosomycin-R: CTTCGCACCAGCACTTCAGACTGG

Eiger-F: AGCGGCGTATTGAGCTGGAG

Eiger-R: TCGTCGTCCGAGCTGTCAAC

Bioinformatic and statistical analysis

Protein alignments were generated by DNAMAN 10.0 (Lynnon Biosoft). All measurement data are expressed as SEM. Comparisons of two samples were made using Student's t test, and multiple samples by ANOVA. Survival curves were compared using the Kaplan–Meier test. P values of less than 0.05 were considered statistically significant. All statistical analyses were performed with GraphPad Prism 9 software. The sample sizes and number of replicates are indicated in the figure legends. Data collection and data analysis were routinely performed by different authors to prevent potential bias. All

318 individuals were included in data analysis.

Figure legends

Figure 1. ORF3a is pathogenic in the nervous system

A. ORF3a localization. *elav.Gal4* and *elav>ORF3a* adult brains labeled for ORF3a (green) and DAPI (blue). ORF3a localized to cytoplasmic foci. **B.** Survival curves of *elav.Gal4* (control) and *elav>ORF3a* adult flies. *elav>ORF3a* median lifespan was significantly less than controls. n>60 flies per genotype. **C.** Longitudinal study of climbing ability. Locomotor activity was reduced in *elav>ORF3a* flies. Each data point represents percent of flies that climbed above 5 cm, averaged for 3 independent trials. See Fig. S1D. **D.** F_1 adult progeny from *elav.gal4,Sb/Tb* X *UAS-ORF3a/Sb* F_0 parents. 3 phenotypic classes with an equivalent number of progeny (33.3%) were expected. *elav>ORF3a* flies were underrepresented. **E.** Micrographs of 3d adult eyes. *GMR>ORF3a* eyes were rough and disorganized. **F.** Stage 16 embryonic body wall muscles labeled with Tropomyosin. *Mef2>ORF3a* embryos showed largely normal body wall musculature (see Fig. S1H for quantification). **G.** Apoptosis assay. *elav.Gal4* and *elav>ORF3a* adult brains labeled for cleaved Caspase-3 (green) and DAPI (blue). ORF3a induced Caspase-3 cleavage. **H.** Immunoblot of whole brain lysates from 3d *elav.Gal4* and *elav>ORF3a* adults validated results shown in (**G**). **I.** qRT-PCR of RNA from 3d old adult heads. Transcripts encoding IMD pathway reporters (*dipt* and *attA*) and a Toll pathway reporter (*Drs*) were enriched in *elav>ORF3a* flies. n>20 unless otherwise noted. Error bars represent standard error of the mean (SEM) from at least three independent replicates. Significance was determined by log-rank test (B), two-way ANOVA (C), and student's t-test (I). *p < 0.05, **p < 0.01, ****p < 0.0001, (ns) non-significant.

Figure S1. Related to Figure 1.

A. Protein alignment of SARS-Cov-ORF3a and SARS-Cov-2-ORF3a. Dark blue shading shows identical residues, light blue shading shows similar residues. **B.** PCR of genomic DNA from ORF3a two independent transgenic lines. ORF3a band is indicated with red arrow. **C.** RT-PCR of *ORF3a* mRNA shows *ORF3a* expression is induced in muscle (*Mef2.Gal4*) and in the nervous system (*GMR.Gal4*). ORF3a band is shown (red arrow). **D.** Representative result of a climbing assay. *elav>ORF3a* flies (right) had reduced motor function. **E.** 6d old female flies. *elav>ORF3a* flies (right) showed severely swollen abdomens. **F.** Survival curves of *Mef2.Gal4* (control) and *Mef2>ORF3a* adult flies. *Mef2>ORF3a* median

lifespan was not significantly different than controls. n>60 flies per genotype. **G.** Longitudinal study of climbing ability. Locomotor activity was unaffected in *Mef2>ORF3a* flies. Each data point represents percent of flies that climbed above 5 cm, averaged for 3 independent trials. **H.** Quantification of embryonic body wall muscle phenotypes from Fig. 1F. Diagram shows the 30 muscles per embryonic segment; blue muscles were 100% normal in >60 *Mef2>ORF3a* embryonic segments, red muscles showed a developmental phenotype in at least 1 of the 60 segments. Dot plot shows frequency of muscle phenotypes is <9.0%. (ns) not significant.

Figure 2. Chloroquine (CQ) protects against ORF3a-induced dysfunction.

A. Survival curves of *elav.Gal4* (control), *elav>ORF3a*, and CQ treated *elav>ORF3a* adult flies. CQ treatment significantly extended *elav>ORF3a* median lifespan. n>60 flies per genotype **B.** Longitudinal study of climbing ability. Locomotor activity was significantly improved in *elav>ORF3a* flies treated with CQ. Each data point represents percent of flies that climbed above 5 cm, averaged for 3 independent trials. **C.** F_1 adult progeny treated with CQ from *elav.gal4,Sb/Tb* X *UAS-ORF3a/Sb* F_0 parents. 3 phenotypic classes with an equivalent number of progeny (33.3%) were expected. CQ treatment improved *elav>ORF3a* survivability to adulthood (compare to Fig. 1D). **D.** Immunoblot of whole brain lysates from 3d *elav.Gal4, elav>ORF3a,* and CQ treated *elav>ORF3a* adults. CQ reduced cleaved Caspase-3 levels in *elav>ORF3a* flies. **E,F.** qRT-PCR of RNA from 3d old adult heads. CQ treatment blunted the expression of the Toll pathway reporter *Drs* (E), but not IMD pathway reporters (*dipt* and *attA*; F) in *elav>ORF3a* flies. **G.** Live imaging of HELA cells transfected with CMV-GFP-ORF3a (green) for 24hr, treated with or without CQ, and labeled with Lysotracker (red). ORF3a transfected cells showed reduced Lysotracker staining (deacidified lysosomes) than untransfected controls (outlined in heat map). CQ treatment restored Lysotracker staining in ORF3a expressing cells **(H)**. n>20 unless otherwise noted. Error bars represent standard error of the mean (SEM) from at least three independent replicates. Significance was determined by log-rank test (A), two-way ANOVA (B), and student's t-test (H). *p < 0.05, **p < 0.01, ****p < 0.0001, (ns) non-significant.

Figure 1 ORF3a is pathogenic in nervous system

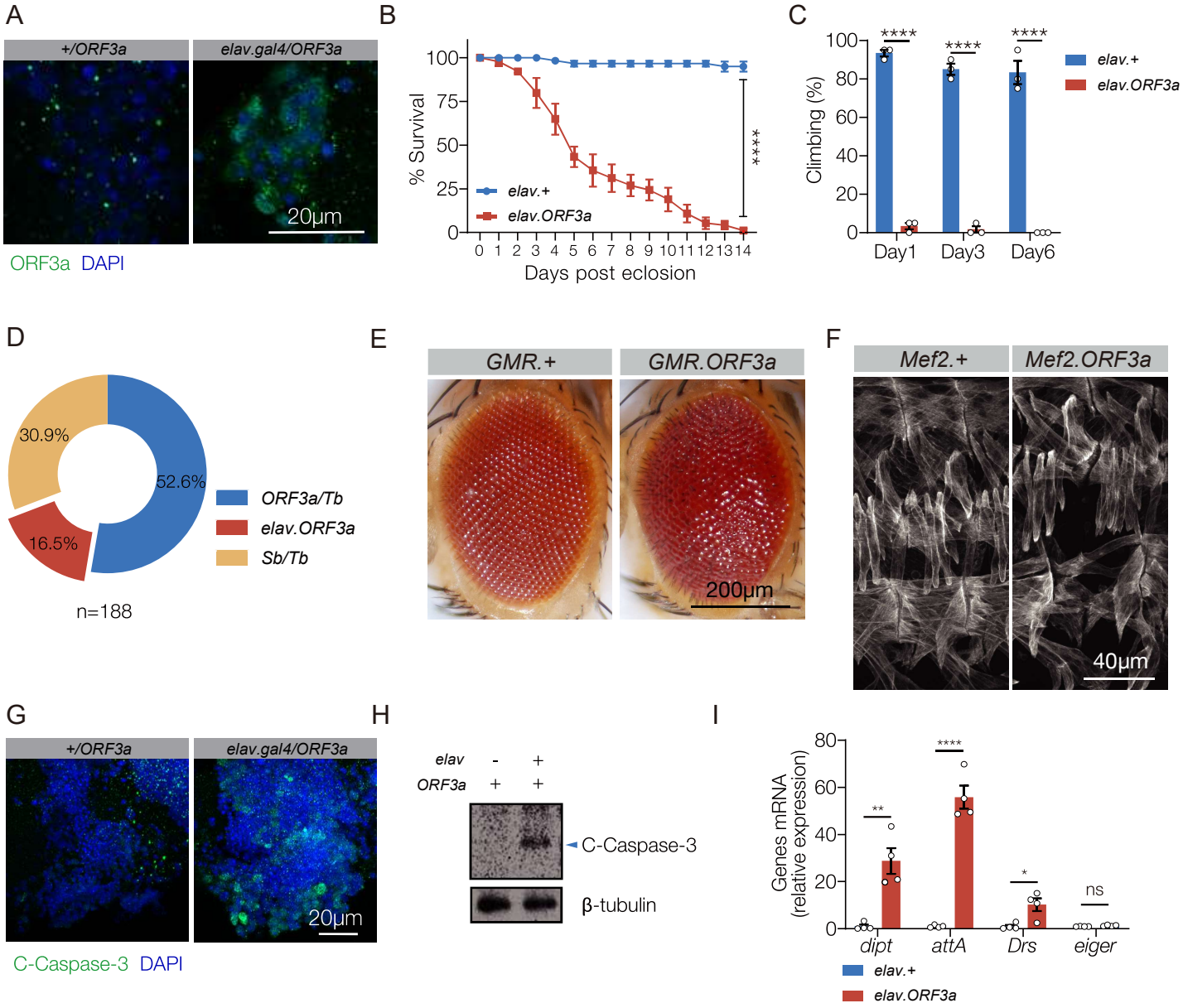

Supplemental Figure 1, related to Figure 1

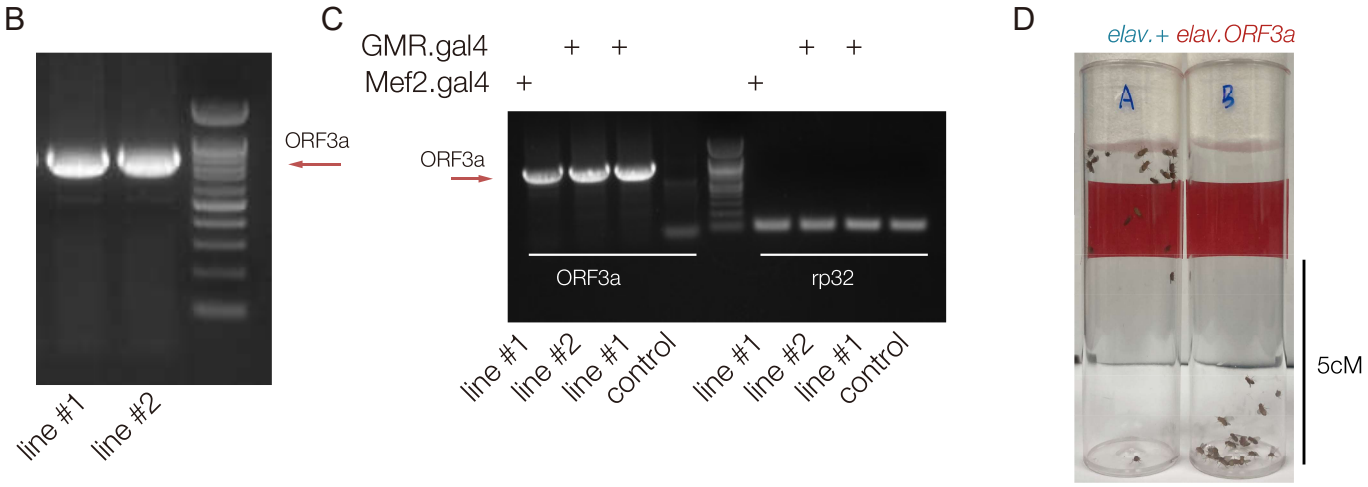

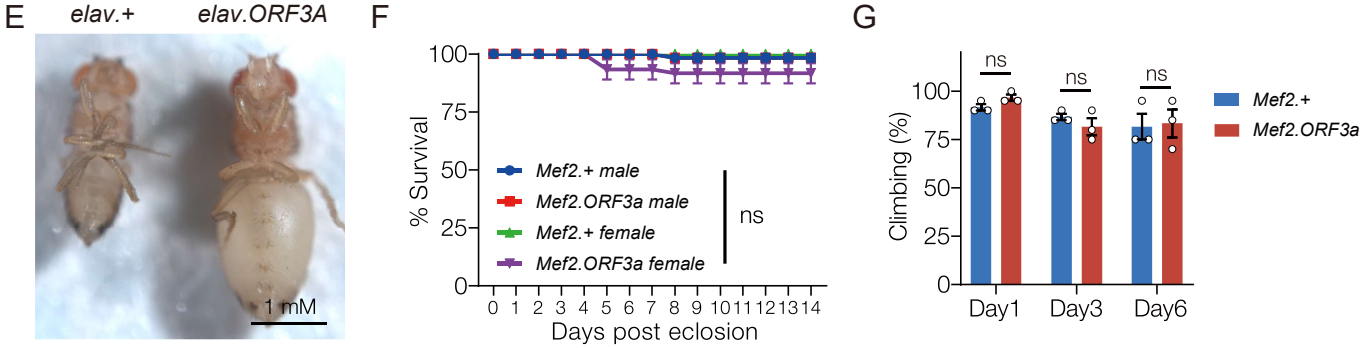

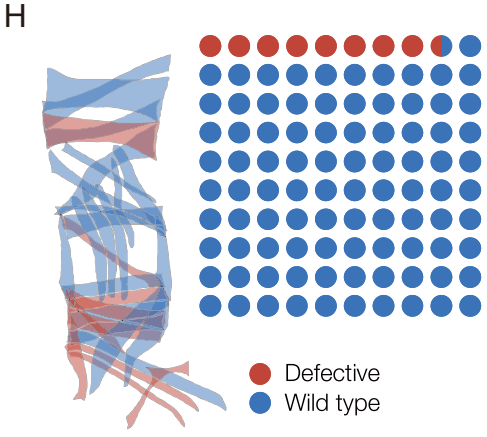

Figure 2 Chloroquine protects against ORF3a induced dysfunction